Communication

A Novel Training-Free Processed Fe-Mn-Si-Cr-Ni Shape Memory Alloy Undergoing $\delta \rightarrow \gamma$ Phase Transformation

HUABEI PENG, GAIXIA WANG, YANGYANG DU, SHANLING WANG, JIE CHEN, and YUHUA WEN

We not only suppress the formation of twin boundaries but also introduce a high density of stacking faults by taking advantage of $\delta \rightarrow \gamma$ phase transformation in a processed Fe-19.38Mn-5.29Si-8.98Cr-4.83Ni shape memory alloy. As a result, its shape memory effect is remarkably improved after heating at 1533 K (1260 °C) (single-phase region of δ ferrite) and air cooling due to $\delta \rightarrow \gamma$ phase transformation.

DOI: 10.1007/s11661-016-3521-8

Low-cost Fe-Mn-Si-based shape memory alloys (SMAs), possessing one-way shape memory effect, have attracted much attention for several decades as a possible alternative to the expensive Ti-Ni-based SMAs.[1–6] A large recovery strain of 9 pct has been reported in a single-crystalline Fe-30Mn-1Si alloy.[1] However, only 2 to 3 pct recovery strain is attained in ordinary polycrystalline-processed Fe-Mn-Si-based alloys without special treatment.[4–6] There are three kinds of special treatment—training,[7–9] thermomechanical,[5,10,11] and ausforming[12,13]—that improve the recovery strain of polycrystalline-processed Fe-Mn-Si SMAs to 4 to 5 pct. The preceding treatments not only increase the production cost, but also make it difficult to fabricate the components with complicated shape. Recently, we manufactured a novel training-free cast Fe-20.2Mn-5.6Si-8.9Cr-5.0Ni alloy by simple synthesis processing, consisting only of casting plus annealing, and made a breakthrough to attain a tensile recovery strain of 7.6 pct in this cast alloy.[14] Nevertheless, there are still shortcomings for cast alloys as compared with processed alloys, *i.e.*, lower recovery stress and worse mechanical properties. Thus, we raise an issue regarding how to obtain training-free processed Fe-Mn-Si-based SMAs.

Recently, we investigated the interaction between twin boundaries and stress-induced ε martensite in Fe-Mn-Si-based SMAs and found that this interaction not only suppresses the stress-induced ε martensitic transformation, but also severely distorts the twin interfaces.[14] As a result, a high density of twin boundaries results in a poor shape memory effect in processed Fe-Mn-Si-based SMAs, and a good shape memory effect could be obtained by inhibiting the formation of twin boundaries. Furthermore, Kajiwara indicated that a high density of stacking faults is beneficial to obtaining a good shape memory effect for processed Fe-Mn-Si-based SMAs.[5] Indeed, the previously mentioned special treatments that effectively improve the shape memory effect introduce the high density of stacking faults besides reducing the twin boundaries for processed Fe-Mn-Si-based SMAs.[5,8,13–15] Here, we also achieve the purpose of both reducing the twin boundaries and introducing the high density of stacking faults using $\delta \rightarrow \gamma$ phase transformation in a Fe-19.38Mn-5.29Si-8.98Cr-4.83Ni alloy. Therefore, in the present article, a novel training-free processed Fe-Mn-Si-Cr-Ni alloy is developed based on $\delta \rightarrow \gamma$ phase transformation.

The ingot of Fe-19.38Mn-5.29Si-8.98Cr-4.83Ni SMA was prepared by induction melting in an argon atmosphere. This ingot was then hot forged at 1373 K (1100 °C) into a 20-mm-thick plate after homogenization at 1373 K (1100 °C) for 15 hours. Three specimens with dimensions of 13 mm × 20 mm × 100 mm were cut from the plate by electric discharge machining and were subsequently solution treated at 1373 K (1100 °C) for 50 minutes, followed by air cooling. Next, two specimens were further heat treated at 1523 K and 1533 K (1250 °C and 1260 °C) for 30 minutes, respectively, followed by air cooling. The preceding heat treatments were accomplished in a high-temperature furnace equipped with a standard alumina-sheathed platinum–rhodium/platinum thermocouple. To evaluate the shape memory effect, wire samples with a cross section of 1.5 mm × 2 mm were cut from the specimens by electric discharge machining. Phase transformation temperatures, *i.e.*, M_s, A_s, and A_f, were measured by electric resistivity–temperature curves. The shape memory effect was determined by the bending technique, as described in Reference 16. Both a homemade mold and the wire specimens were immersed in alcohol and cooled to the deformation temperature by liquid nitrogen before testing the shape memory effect. The specimens were bent at their M_s plus 10 K (10 °C) by the

HUABEI PENG, Associate Professor, GAIXIA WANG, Postgraduate Student, JIE CHEN, Doctoral Candidate, and YUHUA WEN, Professor, are with the College of Manufacturing Science and Engineering, Sichuan University, Chengdu 610065, China. Contact e-mail: wenyh@scu.edu.cn YANGYANG DU, Engineer, is with the Changzhi Qinghua Machinery Factory, Changzhi 046000, China. SHANLING WANG, Associate Professor, is with the Analytical and Testing Center, Sichuan University, Chengdu 610065, China. Contact e-mail: wangshanling@scu.edu.cn

Manuscript submitted September 2, 2015.
Article published online April 29, 2016

homemade mold for 4 pct deformation strain and then recovered by annealing in a muffle furnace at 873 K (600 °C) for 5 minutes. An ordinary optical metallographic method was used to reveal the microstructures undergoing $\delta \rightarrow \gamma$ phase transformation, and its etching solution was 1 mL HF + 15 mL H_2O_2 + 1 g $C_2H_2O_4$ + 15 mL H_2O. A color optical metallographic method was chosen to reveal the residual δ ferrite resulting from $\delta \rightarrow \gamma$ phase transformation, and its etching solution was 1.2 pct $K_2S_2O_5$ + 0.5 pct NH_4HF_2 in distilled water. Microstructures were further studied using a Tecnai G2 F20 transmission electron microscope (TEM) as well as electron backscatter diffraction (EBSD) using a FEI F50 field emission scanning electron microscope. A step size of 1 μm was used to scan the samples for EBSD. The grain size was measured according to the results of EBSD. In the preparation of foils for TEM observations, the specimens were mechanically ground and then polished in a solution of sulfuric acid and methanol (1:4) using a twin jet polisher. Stacking fault probability is in direct proportion to the density of stacking faults. Thus, two austenitic reflections, *i.e.*, $(111)_\gamma$ and $(200)_\gamma$, were detected by a Bruker D8 Advance X-ray diffraction apparatus with Co K_α radiation, and the stacking fault probability was calculated according to the X-ray peak shift method described in Reference 17.

Figure 1 gives the microstructures of solution-treated alloy before and after heating at 1533 K (1260 °C) and air cooling. A high density of twin boundaries exists in solution-treated alloy at 1373 K (1100 °C) for 50 minutes, as seen in the ordinary and color optical micrographs (Figures 1(a) and (b)). For solution-treated alloy after heating at 1533 K (1260 °C) for 30 minutes and air cooling, its microstructure is typical Widmanstätten morphology in the ordinary optical micrograph (Figure 1(c)). Furthermore, a small amount of δ ferrite is distributed in the austenite (Figure 1(d)). When Fe-Mn-Si-Cr-Ni SMAs solidify as ferritic mode, liquid phase first fully transforms into single-phase δ ferrite; then, the austenite nucleates preferentially at δ ferrite grain boundaries and subsequently grows into the δ ferrite by the Widmanstätten mechanism during cooling; finally, their microstructure at room temperature consists of Widmanstätten austenite and residual lathy δ ferrite because of the incomplete nature of $\delta \rightarrow \gamma$ phase transformation.[18,19] Cheng *et al.* also obtained the Widmanstätten structure due to $\delta \rightarrow \gamma$ phase transformation in an austenitic Fe-25.3Mn-4.4Al alloy subjected to heating at 1623 K (1350 °C) for 30 minutes and air cooling, when its high-temperature equilibrium phase is ferrite at 1623 K (1350 °C).[20] Thus, the high equilibrium phase of Fe-19.38Mn-5.29Si-8.98Cr-4.83Ni alloy is δ ferrite at 1533 K (1260 °C), and this alloy underwent $\delta \rightarrow \gamma$ phase transformation during the air-cooling process after heating at 1533 K (1260 °C). In addition, we cannot observe the twin boundaries in solution-treated

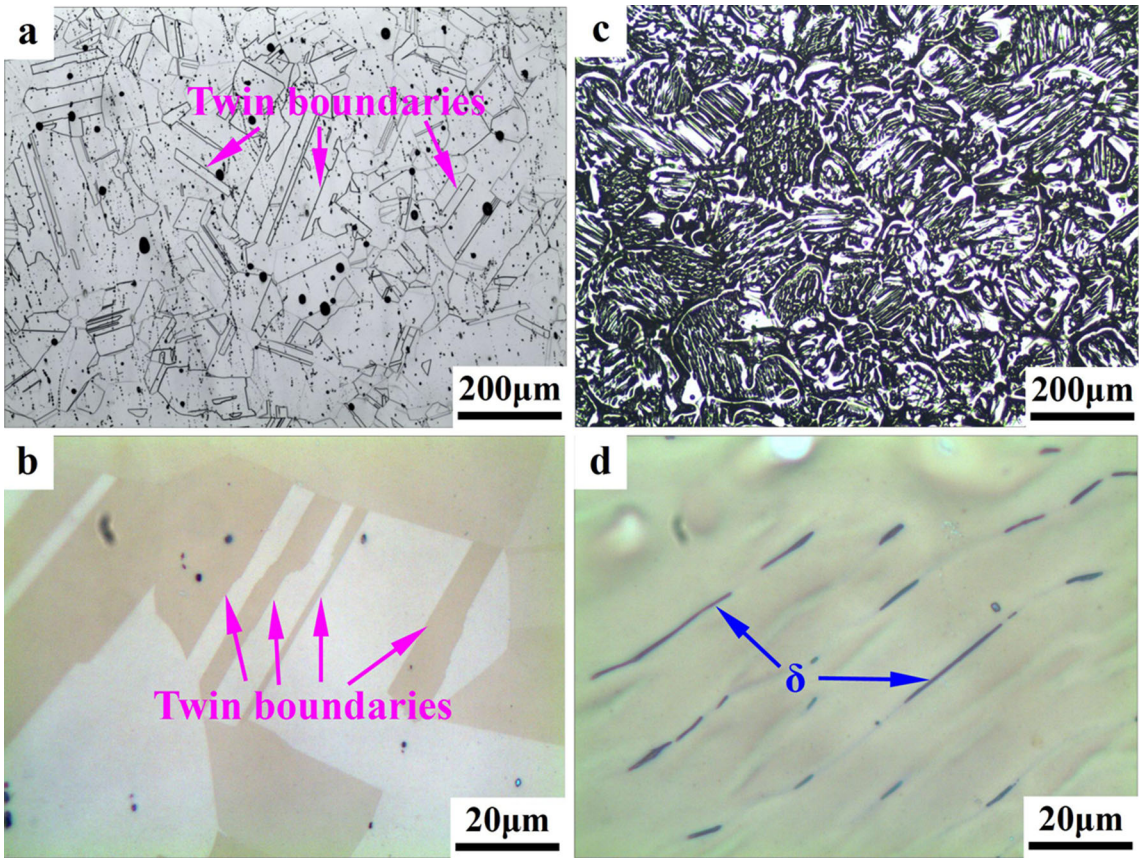

Fig. 1—(*a*) and (*b*) Solution-treated Fe-19.38Mn-5.29Si-8.98Cr-4.83Ni alloy at 1373 K (1100 °C) for 50 min before and after heating at 1533 K (1260 °C) for 30 min and (*c*) and (*d*) air cooling. (a) and (c) are ordinary optical micrographs; (b) and (d) are color optical micrographs.

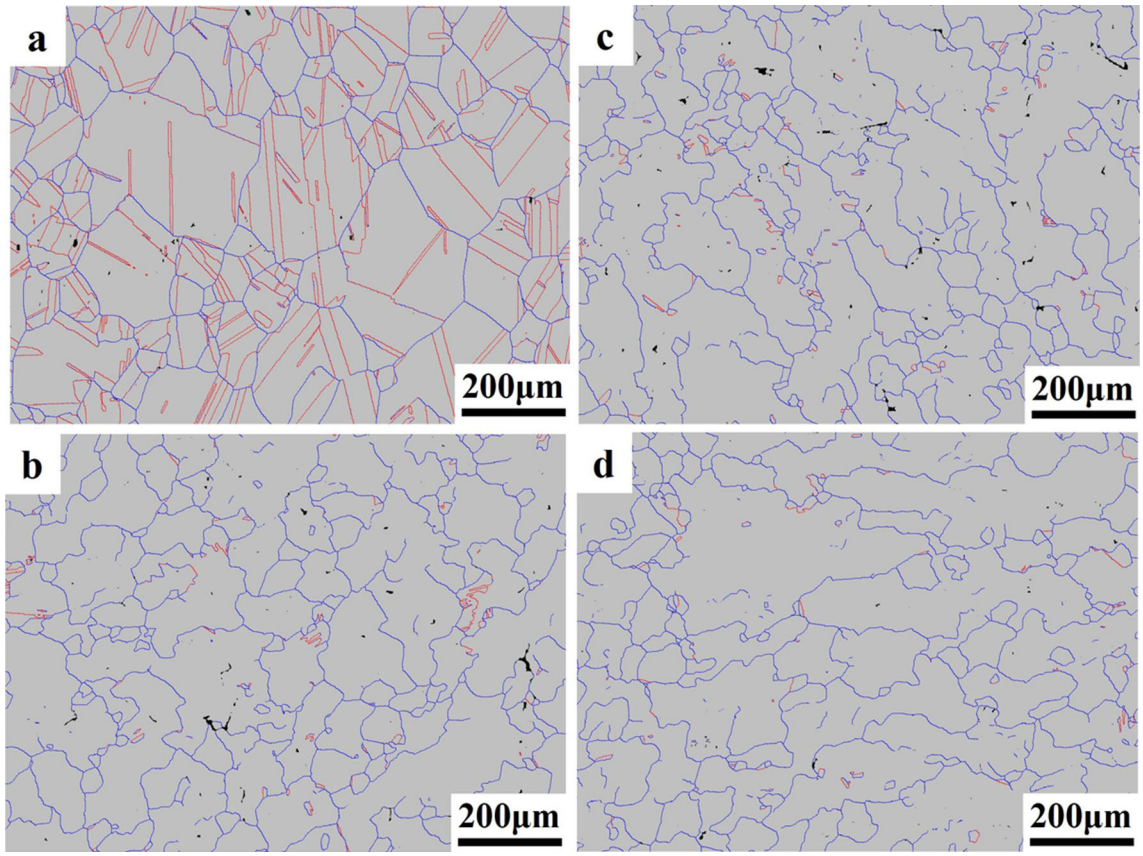

Fig. 2—Austenitic phase maps of (*a*) solution-treated Fe-19.38Mn-5.29Si-8.98Cr-4.83Ni alloy at 1373 K (1100 °C) for 50 min as well as (*b*) one treated at 1533 K (1260 °C) for 30 min and cooled in air and further annealed at (*c*) 873 K (600 °C) and (*d*) 1373 K (1100 °C) for 30 min. Blue lines are grain boundaries, while red lines are twin boundaries (Color figure online).

alloy after heating at 1533 K (1260 °C) and air cooling according to the results of optical micrographs.

We further used EBSD to quantitatively determine the length fraction of twin boundaries, *i.e.*, the ratio of the total length of the twin boundaries to the total length of all grain boundaries (>15 deg), including the twin boundaries (Figure 2; Table I). For solution-treated alloy at 1373 K (1100 °C) for 50 minutes, the length fraction of twin boundaries reached 55.4 pct (Figure 2(a)). Note that the length fraction of twin boundaries was observed to decrease to 8.7 pct when this alloy was further heated at 1533 K (1260 °C) for 30 minutes and cooled in air (Figure 2(b)). The preceding results indicate that heating at 1533 K (1260 °C) and air cooling is an effective heating treatment to suppress the formation of twin boundaries. In other words, we can use $\delta \rightarrow \gamma$ phase transformation to realize the purpose of suppressing the formation of twin boundaries through heating the Fe-Mn-Si-based SMAs to the δ ferrite phase region. Moreover, the length fractions of twin boundaries are only 8.0 pct (Figure 1(c)) and 5.7 pct (Figure 1(d)) when this alloy undergoing $\delta \rightarrow \gamma$ phase transformation was further annealed at 873 K (600 °C) and 1373 K (1100 °C) for 30 minutes, respectively. As a result, it is difficult to introduce the twin boundaries by subsequent annealing treatments for the Fe-Mn-Si-Cr-Ni alloy undergoing $\delta \rightarrow \gamma$ phase transformation.

Annealing twins have been observed in a variety of fcc metals and alloys with intermediate or low stacking fault energy after deforming and subsequent annealing.[21–23] In the present article, the Fe-19.38Mn-5.29Si-8.98Cr-4.83Ni alloy was subjected to hot forging at 1373 K (1100 °C) and subsequent solution treating at 1373 K (1100 °C). Obviously, the twin boundaries (Figure 2(a)) are annealing twins for solution-treated Fe-19.38Mn-5.29Si-8.98Cr-4.83Ni alloy. Generally, it is difficult to control the distribution and configurations of annealing twins. Mahajan indicated that annealing twins form due to growth accidents on differently inclined {111} facets present on a migrating grain boundary.[23] It is emphasized that grain boundary migration is an essential component for the formation of annealing twins.[21,23] For solution-treated alloy after heating at 1533 K (1260 °C), the migrating interfaces are mainly γ/δ interfaces rather than grain boundaries due to $\delta \rightarrow \gamma$ phase transformation during the air-cooling process. In this case, $\delta \rightarrow \gamma$ phase transformation is successful to suppress the formation of twin boundaries. Thus, the length fraction of twin boundaries markedly decreased from 55.4 to 8.7 pct for solution-treated alloy after heating at 1533 K (1260 °C) and air cooling (Figures 2(a) and (b)). When the alloy undergoing $\delta \rightarrow \gamma$ phase transformation was further annealed at 873 K or 1373 K (600 °C or 1100 °C), the grain size increased slightly with the

Table I. Grain Size, Phase Transformation Temperatures, Twin Boundaries, Stacking Fault Probability, and Shape Recovery Ratio of Fe-19.38Mn-5.29Si-8.98Cr-4.83Ni Alloy After Different Heating Treatments

Heating Treatments	Grain Size (μm)	Phase Transformation Temperatures			Length Fraction of Twin Boundaries (Percent)	Stacking Fault Probability	Shape Recovery Ratio (Percent)
		M_s	A_s	A_f			
1373 K (1100 °C) × 50 min	107.7 ± 32.8	215 K (−58 °C)	338 K (65 °C)	363 K (90 °C)	55.4	0.0183	63
1523 K (1250 °C) × 30 min	128.7 ± 43.1	228 K (−45 °C)	333 K (60 °C)	379 K (106 °C)	53.1	—	64
1533 K (1260 °C) × 30 min	108.6 ± 38.3	226 K (−47 °C)	328 K (55 °C)	370 K (97 °C)	8.7	0.0260	81
1533 K (1260 °C) × 30 min plus 873 K (600 °C) × 30 min	115.4 ± 35.5	218 K (−55 °C)	331 K (58 °C)	388 K (115 °C)	8.0	0.0229	90
1533 K (1260 °C) × 30 min plus 1373 K (1100 °C) × 30 min	124.3 ± 36.9	241 K (−32 °C)	343 K (70 °C)	381 K (108 °C)	5.7	0.0179	76

annealing temperatures (Table I) and the morphology of grains was almost the same before and after annealing (Figure 2). This result means that the grain boundary migration is limited; thus, the twin boundaries are hardly introduced by annealing. The reason for limited grain boundary migration may be attributed to the pinning effect of residual δ ferrite resulting from the incomplete nature of $\delta \rightarrow \gamma$ phase transformation.

In order to further demonstrate that $\delta \rightarrow \gamma$ phase transformation can suppress the formation of twin boundaries, we investigated the microstructure of solution-treated alloy after heating at 1523 K (1250 °C) for 30 minutes and air cooling (Figure 3). Many islandlike Widmanstätten structures are distributed uniformly in the white structures, and some twin boundaries appear in the white structures (Figure 3(a)). The color optical micrograph reveals that the islandlike Widmanstätten structures consist of austenite and δ ferrite (Figure 3(b)). Obviously, the islandlike Widmanstätten areas are δ ferrite at 1523 K (1250 °C) and resulted from the $\delta \rightarrow \gamma$ phase transformation during the air-cooling process after heating at 1523 K (1250 °C). Therefore, the high equilibrium phases of Fe-19.38Mn-5.29Si-8.98Cr-4.83Ni alloy consist of austenite and δ ferrite at 1523 K (1250 °C). According to the preceding typical microstructure, we determined the volume fraction of δ ferrite at 1523 K (1250 °C) by measuring the islandlike Widmanstätten areas of seven micrographs. The results show that the volume fraction of δ ferrite is 72.9 pct, while that of austenite is 27.1 pct at 1523 K (1250 °C). Note that the morphology of twin boundaries after heating at 1523 K (1250 °C) and air cooling is different from that of solution-treated alloy, and few twin boundaries are observed in the areas around δ ferrite (Figures 3(c) and (d)). The δ ferrite results from the incomplete nature of $\delta \rightarrow \gamma$ phase transformation; thus, the areas around δ ferrite are subjected to $\delta \rightarrow \gamma$ phase transformation. In this case, the preceding results further demonstrate that $\delta \rightarrow \gamma$ phase transformation is effective in inhibiting the formation of twin boundaries. However, the length fraction of twin boundaries still reaches up to 53.1 pct for this alloy undergoing $\delta \rightarrow \gamma$ phase transformation (Table I). There is the retained austenite of 27.1 pct at 1523 K (1250 °C), and the twin boundaries also exist in the retained austenite. Furthermore, these pre-existing twin boundaries in the retained austenite may further grow along the migrating interfaces of γ/δ during the air-cooling process after heating at 1523 K (1250 °C). As a result, heating in the two-phase region of austenite and δ ferrite cannot effectively inhibit the formation of twin boundaries through $\delta \rightarrow \gamma$ phase transformation.

The microstructures undergoing $\delta \rightarrow \gamma$ phase transformation before and after annealing were further investigated with a TEM (Figure 4). Generally, a relatively low density of stacking faults appears in Fe-Mn-Si-based SMAs subjected to solution treatment at around 1273 K (1000 °C).[24–26] Note that there are many stacking faults and a certain amount of dislocations (red arrows) distributed in the austenite for solution-treated alloy after heating at 1533 K (1260 °C) for 30 minutes and air cooling (Figure 4(a)). This result indicates that $\delta \rightarrow \gamma$ phase transformation is

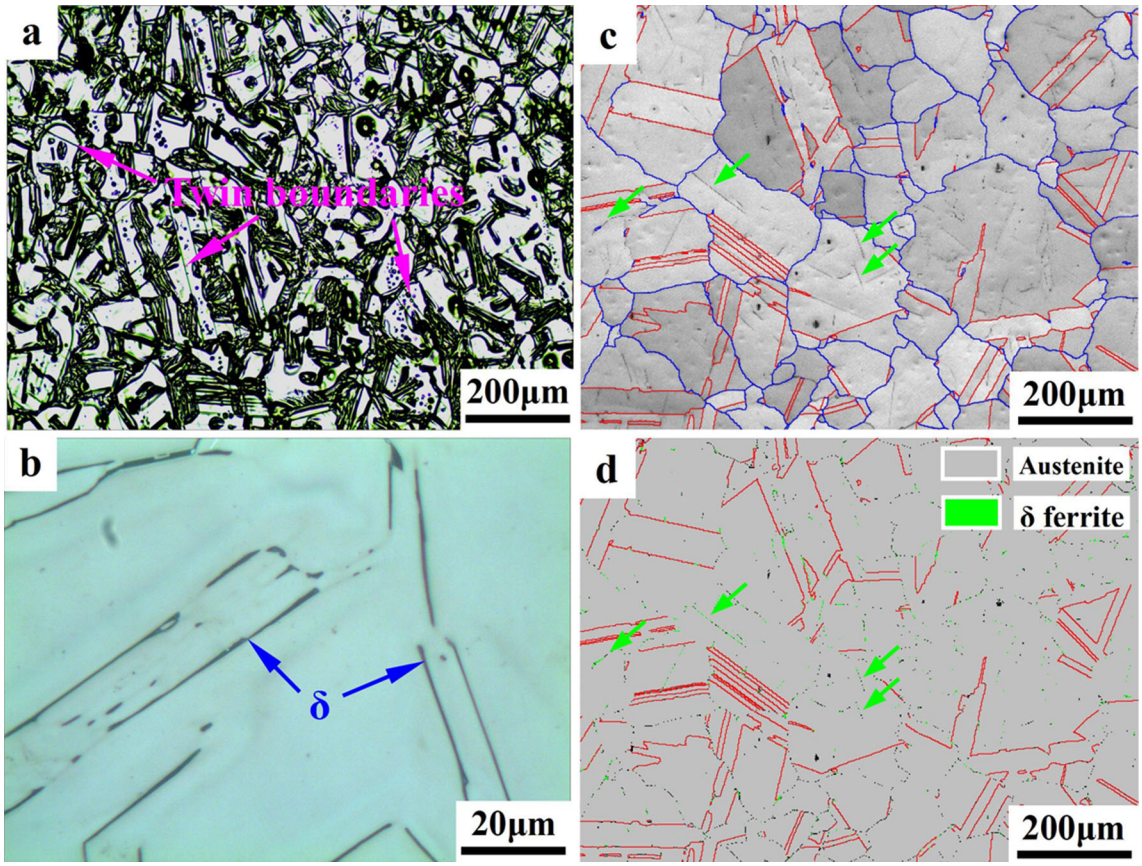

Fig. 3—(*a*) Ordinary and (*b*) color optical micrographs as well as (*c*) image quality map and (*d*) phase map of solution-treated Fe-19.38Mn-5.29-Si-8.98Cr-4.83Ni alloy after heating at 1523 K (1250 °C) for 30 min and air cooling. (c) and (d) Blue lines are grain boundaries, while red lines are twin boundaries (Color figure online).

beneficial to inducing the defects, especially stacking faults. It is well known that the proper heating treatment can eliminate the defects, such as stacking faults and dislocations. As a result, numerous stacking faults still existed, while a few dislocations remained after further annealing at 873 K (600 °C) for 30 minues (Figure 4(b)). When annealed at 1373 K (1100 °C) for 30 minutes, the amount of stacking faults reduced and few dislocations remained (Figure 4(c)). The results of stacking fault probability further verify the preceding TEM results (Table I).

Solid-phase transformation-induced defects have been reported in various metals and alloys, *i.e.*, $\gamma \rightarrow \alpha$[27,28] or $\delta \rightarrow \gamma$ phase transformation[29–33] induced defects in Fe-based alloys. Two factors are responsible for the generation of defects: plastic deformation induced by volume and shape changes as well as growth accidents.[32–34] The phase transformation from δ ferrite to the austenite causes volume shrinkage of about 1 pct.[32] Moreover, the δ ferrite is harder than the austenite. As a result, the plastic deformation has to be induced in the soft austenite in order to release about 1 pct volume change. The defects, therefore, are introduced into the austenite. This is one reason for the stacking faults and dislocations induced by $\delta \rightarrow \gamma$ phase transformation for solution-treated alloy after heating at 1533 K (1260 °C) and air cooling (Figure 4(a)). Note that growth accidents are another reason for the preceding defects induced by $\delta \rightarrow \gamma$ phase transformation. During the migration of interfaces between parent and new phases, atoms are removed from the side of the parent phase at the interfaces and are added to the side of the new phase. Growth accidents may happen if these atoms are not placed on the lattice of the growing new phase according to the proper stacking sequence.[34–36] As a result, defects would be introduced into the new phase by the growth accidents. In the case of $\delta \rightarrow \gamma$ phase transformation, the γ/δ interfaces migrate into the δ ferrite by the transfer of atoms from δ ferrite. Growth accidents will occur since an atom plane containing a row of atoms displaced from the sites occupies the perfect lattice. In this case, the empty channels are too narrow to accommodate another row of atoms. If the next atom plane resumes the original stacking sequence, the defects will be induced.

As mentioned previously, both reducing the twin boundaries and introducing the high density of stacking faults are beneficial for improving the shape memory effect in Fe-Mn-Si-based SMAs. Note that we both suppressed the formation of twin boundaries and introduced the high density of stacking faults using $\delta \rightarrow \gamma$ phase transformation in solution-treated alloy after heating at

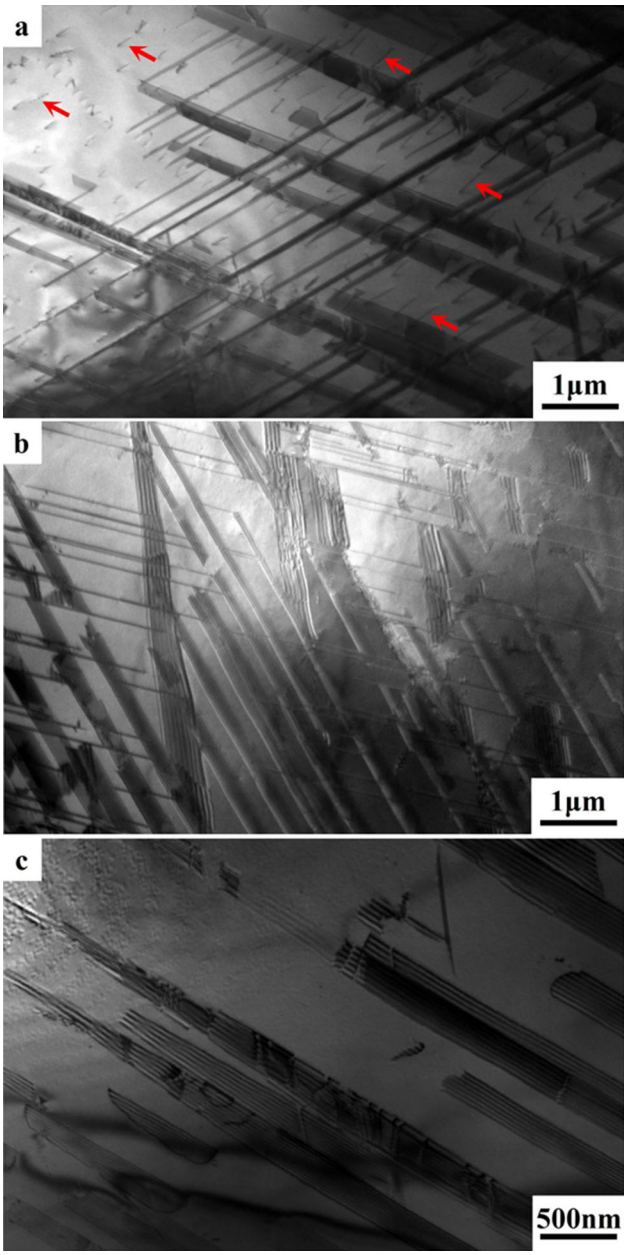

Fig. 4—(a) TEM micrographs of solution-treated Fe-19.38Mn-5.29-Si-8.98Cr-4.83Ni alloy after heating at 1533 K (1260 °C) for 30 min and air cooling as well as subsequent annealing at (b) 873 K (600 °C) and (c) 1373 K (1100 °C) for 30 min.

1533 K (1260 °C) and air cooling. As a result, the alloy's shape recovery ratio was significantly improved to 81 pct from the solution-treated state of 63 pct when the deformation strain was 4 pct and the deformation temperature was M_s plus 10 K (10 °C) (Table I). After being subsequently annealed at 873 K (600 °C), the alloy's shape recovery ratio further increased to 90 pct due to the reduction in the dislocations, which inhibit the stress-induced ε-martensitic transformation.[13,37–39] On the contrary, after being subsequently annealed at 1373 K (1100 °C), the alloy's shape recovery ratio decreased to 76 pct because of the reduction in the amount of stacking faults, which are beneficial to stress-induced ε-martensitic transformation.[5] For solution-treated alloy after heating at 1523 K (1250 °C) and air cooling, a high density of twin boundaries, which has a negative effect on the shape memory effect, still existed (Figure 3). In this case, the alloy's shape recovery ratio was only 64 pct.

In conclusion, we developed a novel training-free processed Fe-19.38Mn-5.29Si-8.98Cr-4.83Ni alloy using $\delta \rightarrow \gamma$ phase transformation. The shape memory effect could be remarkably improved by using $\delta \rightarrow \gamma$ phase transformation upon heating at a single-phase region of δ ferrite. However, $\delta \rightarrow \gamma$ phase transformation exhibits no positive effect on improving the shape memory effect upon heating at the two-phase region of δ ferrite and austenite. Accordingly, heating at the δ phase region and subsequent use of $\delta \rightarrow \gamma$ phase transformation is a novel idea for developing training-free processed Fe-Mn-Si-based SMAs. It holds great promise for further improvement of the shape recovery effect through modifying and optimizing the heat treatments. Our results will further promote the application of Fe-Mn-Si-based SMAs in engineering areas. In addition, to our knowledge, an equilibrium phase diagram for Fe-Mn-Si-based SMAs has not yet been developed. Our previous study also showed that it is invalid to calculate the equilibrium phase diagram of Fe-(12-30)Mn-5.5Si-8.5Cr-5Ni alloys using THERMO-CALC® software together with database TCFE6.[18] Therefore, the prediction of the δ-phase region for using $\delta \rightarrow \gamma$ phase transformation to fabricate training-free processed Fe-Mn-Si-based SMAs is a critical issue.

We acknowledge the financial support of the National Natural Science Foundation of China (Grant Nos. 51271128 and 51401136).

REFERENCES

1. A. Sato, E. Chishima, K. Soma, and T. Mori: *Acta Metall.*, 1982, vol. 30, pp. 1177–83.
2. A. Sato, E. Chishima, Y. Yamaji, and T. Mori: *Acta Metall.*, 1984, vol. 32, pp. 539–47.
3. A. Sato, Y. Yamaji, and T. Mori: *Acta Metall.*, 1986, vol. 34, pp. 287–94.
4. H. Otsuka, H. Yamada, T. Maruyama, H. Tanahashi, S. Matsuda, and M. Murakami: *ISIJ Int.*, 1990, vol. 30, pp. 674–79.
5. S. Kajiwara: *Mater. Sci. Eng. A*, 1999, vols. 273–275, pp. 67–88.
6. J. Mohd Jani, M. Leary, A. Subic, and M.A. Gibson: *Mater. Des.*, 2014, vol. 56, pp. 1078–1113.
7. Y. Watanabe, Y. Mori, and A. Sato: *J. Mater. Sci.*, 1993, vol. 28, pp. 1509–14.
8. S. Kajiwara and K. Ogawa: *Mater. Sci. Forum*, 2000, vols. 327–328, pp. 211–14.
9. Y.H. Wen, M. Yan, and N. Li: *Mater. Lett.*, 2004, vol. 58, pp. 899–902.
10. N. Stanford and D.P. Dunne: *Mater. Sci. Eng. A*, 2006, vol. 422, pp. 352–59.
11. C.H. Yang, H.C. Lin, K.M. Lin, and H.K. Tsai: *Mater. Sci. Eng. A*, 2008, vol. 497, pp. 445–50.
12. L.J. Rong, Y.Y. Li, and C.X. Shi: *Scripta Mater.*, 1996, vol. 34, pp. 993–98.

13. D. Wang, D. Liu, Z. Dong, W. Liu, and J. Chen: *Mater. Sci. Eng. A*, 2001, vol. 315, pp. 174–79.
14. Y.H. Wen, H.B. Peng, D. Raabe, I. Gutierrez-Urrutia, J. Chen, and Y.Y. Du: *Nat. Commun.*, 2014, vol. 5, p. 4964.
15. D. Liu, S. Kajiwara, T. Kikuchi, N. Shinya, D. Wang, and W. Liu: *Mater. Trans.*, 2000, vol. 41, pp. 593–96.
16. Y.H. Wen, H.B. Peng, C.P. Wang, Q.X. Yu, and N. Li: *Adv. Eng. Mater.*, 2011, vol. 13, pp. 48–56.
17. Y. Rong, G. He, Z. Guo, S. Chen, T.Y. Hsu, and X. Zuyao: *J. Mater. Sci. Technol.*, 2002, vol. 18, pp. 459–61.
18. H.B. Peng, Y.H. Wen, Y.Y. Du, Q.X. Yu, and Q. Yang: *Metall. Mater. Trans. B*, 2013, vol. 44B, pp. 1137–43.
19. H.B. Peng, Y.H. Wen, Y.Y. Du, J. Chen, and Q. Yang: *Metall. Mater. Trans. B*, 2014, vol. 45B, pp. 6–11.
20. W.C. Cheng and C.K. Lai: *Scripta Mater.*, 2006, vol. 55, pp. 783–86.
21. S. Mahajan, C.S. Pande, M.A. Imam, and B.B. Rath: *Acta Mater.*, 1997, vol. 45, pp. 2633–38.
22. C.S. Pande, B.B. Rath, and M.A. Imam: *Mater. Sci. Eng. A*, 2004, vol. 367, pp. 171–75.
23. S. Mahajan: *Scripta Mater.*, 2013, vol. 68, pp. 95–99.
24. C.L. Li and Z.H. Jin: *J. Mater. Eng. Perform.*, 1998, vol. 7, pp. 617–20.
25. H.B. Peng, Y.H. Wen, L.R. Xiong, and N. Li: *Mater. Sci. Eng. A*, 2008, vol. 497, pp. 61–64.
26. A. Druker, A. Baruj, and J. Malarría: *Mater. Charact.*, 2010, vol. 61, pp. 603–12.
27. M.J. Roberts: *Metall. Trans.*, 1970, vol. 1, pp. 3287–94.
28. E.A. Wilson and S.H. Chong: *Metall. Mater. Trans. A*, 2002, vol. 33A, pp. 2425–31.
29. N. Suutala, T. Takalo, and T. Moisio: *Metall. Trans. A*, 1979, vol. 10A, pp. 1183–90.
30. J. Singh, G.R. Purdy, and G.C. Weatherly: *Metall. Trans. A*, 1985, vol. 16A, pp. 1363–69.
31. J.W. Fu and Y.S. Yang: *Mater. Lett.*, 2012, vol. 81, pp. 177–80.
32. H. Yasuda, T. Nagira, M. Yoshiya, A. Sugiyama, N. Nakatsuka, M. Kiire, M. Uesugi, K. Uesugi, K. Umetani, and K. Kajiwara: *IOP Conf. Ser. Mater. Sci. Eng.*, 2012, vol. 33, p. 012036.
33. A. Ramazani, K. Mukherjee, A. Schwedt, P. Goravanchi, U. Prahl, and W. Bleck: *Int. J. Plast.*, 2013, vol. 43, pp. 128–52.
34. H.I. Aaronson, S. Mahajan, G.R. Purdy, and M.G. Hall: *Metall. Mater. Trans. A*, 2002, vol. 33A, pp. 2347–51.
35. G. Bäro and J.H. Perepezko: *Mater. Sci. Eng.*, 1977, vol. 28, pp. 243–48.
36. A.H. King: *Phys. Status Solidi A*, 1983, vol. 76, pp. 629–36.
37. W. Zhang, N. Li, and Y.H. Wen: *Metall. Mater. Trans. B*, 2007, vol. 38B, pp. 299–303.
38. S. Suzuki, S. Senoo, T. Maruyama, and K. Shinoda: *Mater. Trans.*, 2008, vol. 49, pp. 2755–60.
39. S. Senoo, K. Shinoda, M. Sato, T. Maruyama, and S. Suzuki: *Mater. Trans.*, 2008, vol. 49, pp. 1229–34.